The Ground and Excited State Electronic Structures of Ruthenium Quinones and Related Species.

by A. B. P. Lever*, H. Masui, R. A. Metcalfe, D. J. Stufkens[a], E. S. Dodsworth, and P. R. Auburn

Dept. of Chemistry, York University, 4700 Keele St., North York, Ontario, Canada, M3J 1P3, and the Anorganisch Chemisch Laboratorium,[a] Universiteit van Amsterdam, Nieuwe Achtergracht 166, 1018 WV Amsterdam, The Netherlands.

Abstract

Electronic and resonance Raman spectroscopy are used to probe the electronic structures of bipyridine ruthenium complexes of quinone and a series of derivatives in which the oxygen atoms of quinone are successively replaced by NH. The electronic structures of some benzoquinonediimine species are probed by variation of substituent in the benzene ring, and the properties of a diaminophenyl substituted benzoquinonediimine are explored as a function of the twist at the 1,1'-link.

1. Introduction

In 1986 we published the first of a series of reports of the chemistry of ruthenium quinone complexes [1–4]. Consider first the species $[Ru(bpy)_2(L(O.O))]^{n+}$ where bpy = 2,2'-bipyridine and (L(O.O)) may be catechol dianion (Cat), o-benzosemiquinone anion (Sq) or o-benzoquinone (Q), which forms a redox series (Figure 1) in which (L(O.O)) may exist in any of the aforesaid oxidation states, and ruthenium may formally be present as Ru(II) or Ru(III). We are concerned with how one may define the electron distribution in such systems given that both the metal and ligand are redox active. This question has also been raised extensively by the Pierpont laboratory studying closely related systems [5–8]. In this paper we deal with some questions raised as a result of the study of the formally Ru(II) quinone species, $[Ru(bpy)_2Q]^{2+}$.

Initially we were interested in the question of possible intramolecular delocalisation between the limiting electronic structures:

$$[Ru(II)(bpy)_2Q]^{2+} \Longleftrightarrow [Ru(III)(bpy)_2Sq]^{2+} \tag{1}$$

Was it reasonable to assign a specific oxidation state to these species, or not ? As the problem has developed, the answer to this question has become more precise, as is outlined in this report. The programme began with benzoquinones where both coordinating atoms are oxygen (labelled L(O.O)), and progressed to the analogous systems aminophenol (L,NH.O) and benzoquinonediimine (L,NH.NH), both of which may also formally exist in three oxidation states but with further complexity involving the number of protons. The resulting complexes all have the same general formula written in their formally ruthenium(II) oxidation state, as $[Ru(II)(bpy)_2(Q(O.O))]^{2+}$ where $(Q(O.O))$ may be replaced by $(Q(NH.O))$ or $(Q(NH.NH))$. Figure 2 shows part of an MO diagram appropriate for these species (assuming C_{2v} symmetry). One d orbital on the metal, d_{yz} in framework shown, interacts strongly with the ligand LUMO, forming the pair of orbitals $1b_2$ and $2b_2*$. The other two orbitals, $d_{xy}(a_2)$ and $d_{z^2}(a_1)$ are believed to be weakly $\pi*$ and $\sigma*$ respectively; for the purpose of this argument let us assume they are mainly non-bonding. An assessment of the formal oxidation state description of this species then depends, to a rough approximation, upon the question of whether the $1b_2$ electrons are mainly metal, mainly ligand or midway according to:
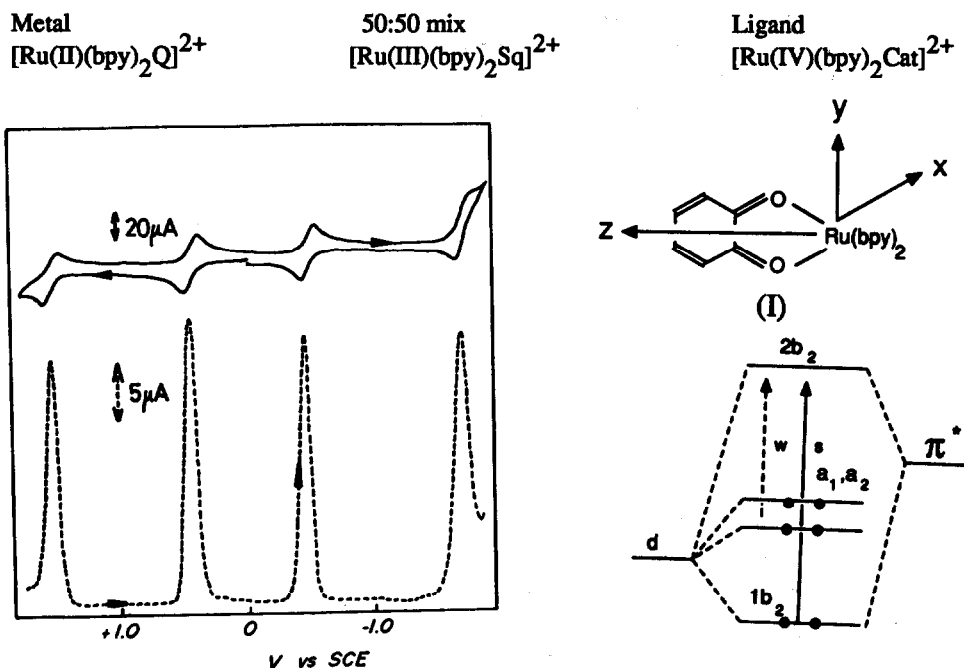
Metal   50:50 mix   Ligand
$[Ru(II)(bpy)_2Q]^{2+}$ $[Ru(III)(bpy)_2Sq]^{2+}$ $[Ru(IV)(bpy)_2Cat]^{2+}$

Figure 1. (Left) Electrochemistry of Ru(bpy)$_2$(DTBCat) in 1,2-dichloroethane. Upper; cyclic voltammogram at 200 mV/s, lower; differential pulse voltammogram at 5 mV/s. Adapted from [1]. DTBCat = 3,5-di-t-butylcatechol.
Figure 2. (Right) A partial molecular orbital diagram showing the interaction of the "t_{2g}" electrons on Ru with the ligand $\pi*$ orbital.

2. Electrochemistry and Electronic Spectra

All three complexes participate in a redox series (Figure 1) which may, generally, and in part, be written:

$$[Ru(III)(bpy)_2Q]^{3+} \xrightarrow{e^-} [Ru(II)(bpy)_2Q]^{2+} \xrightarrow{e^-} [Ru(II)(bpy)_2Sq]^{+} \xrightarrow{e^-} [Ru(II)(bpy)_2Cat] \quad (2)$$
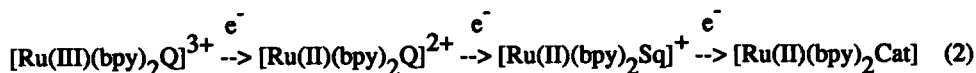
Table 1 shows electrochemical data indicating just how much more readily the (NH.NH) species is oxidisable revealing thereby the greater electron richness of the (NH.NH) coordination sites relative to (O.O)

Figure 3 shows how the principal visible region absorption band, formally identified as the $1b_2 \longrightarrow 2b_2^*$ transition (in Figure 2) of this group of compounds shifts to the blue in the sequence Q = (O.O) < (NH.O) < (NH.NH). This would most easily be ascribed to behaviour of a charge transfer band, Ru(II) $\longrightarrow$ Q(π^*) in a formally divalent $[Ru(II)(bpy)_2Q]^{2+}$ species. However, as we develop this chemistry it is apparent that such an assignment is too simplistic. Let us now consider each species, as a function of ligating atoms, in more detail.
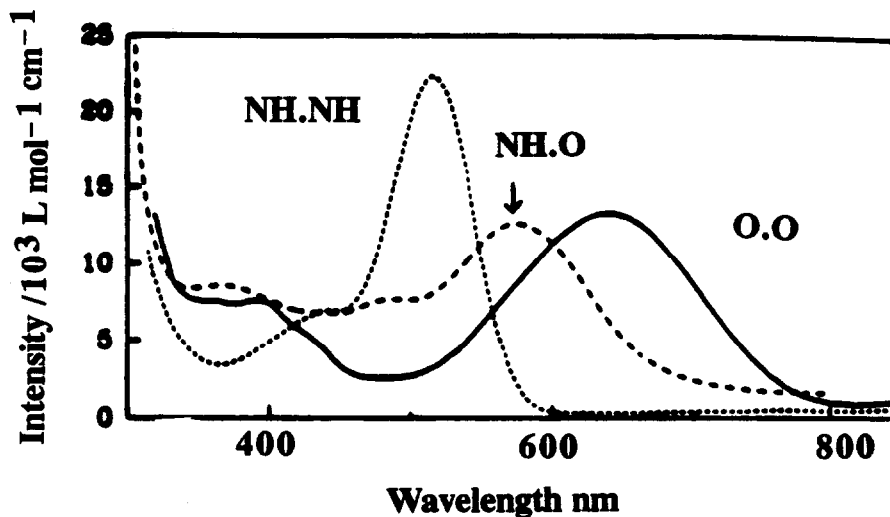

Figure 3. The electronic spectra of $[(bpy)_2RuQ]^{2+}$ species as identified. The (O.O) and (NH.O) species were recorded in 1,2-dichloroethane and the (NH.NH) in acetonitrile. Adapted from [9].

Table 1.
Electrochemical Half-wave Potentials (V vs SCE) for $[(bpy)_2Ru(Q)]^{2+}$ and
Related Systems [9].

Ligand	Ru(III)/Ru(II)[a]	Q/Sq[a]	Sq/Cat[a]
L(O.O)	1.65	0.56	-0.33
L(NH.O)	1.48	0.05	-0.70
L(NH.NH)	1.35	-0.47	-1.15

a) Limiting descriptions in the absence of significant metal-ligand mixing.

3. $[Ru(bpy)_2(L(O.O))]^{2+}$ (I) [1]

The electronic spectrum of this species, (I), shows a strong band at about 19,000 cm^{-1}
(Figure 3). The resonance Raman spectrum exciting into the blue edge [10] of this absorption
band reveals enhancement of both internal quinone vibrations and ν(Ru-O) with the latter of
much greater intensity. This indicates some charge transfer character to the transition but also
implies significant mixing of metal and ligand orbitals. It does not identify whether the band is
ligand to metal (LMCT) or metal to ligand charge transfer (MLCT).

Some evidence points to the Ru(II)Q description as most appropriate, namely:

i) The analogous $[Ru(NH_3)_4(L(O.O))]^{2+}$ species has an FTIR spectrum, consistent
with the presence of a quinone ligand [11].
ii) The band near 400 nm (Figure 3) is fully consistent with a Ru(II) ---> π*bpy
transition [1,10,12].
iii) The $1b_2$ ---> $2b_2$* transition behaves like an MLCT transition in shifting to the
blue in the sequence (L(O.O)) < (L(NH.O)) < (L(NH.NH)).

However there are problems with this view since some observations point towards an
Ru(III) formulation, namely:

i) In comparing the electronic spectra of $[Ru(bpy)_2(DTBQ(O.O))]^{2+}$ and
$[Ru(bpy)_2(TClQ(O.O))]^{2+}$ (DTBQ(O.O) = 3,5-di-t-butylbenzoquinone, TClQ(O.O) =
tetrachloroquinone) the $1b_2$ ---> $2b_2$* band shifts like an LMCT rather than an MLCT band
[1].
ii) The osmium analogue is almost certainly $[Os(III)(bpy)_2Sq(O.O)]^{2+}$ [8] on the
basis, inter alia, that a band is observed in the near infrared spectrum probably assignable to
an intraconfigurational t_{2g}^5 transition. iii) In the spectrum of the related complex
$[Ru(NH_3)_4(L(O.O))]^{2+}$, the $1b_2$ ---> $2b_2$* transition lies at <u>higher</u> energy than in the

bipyridine analogue yet the $[Ru(II)(NH_3)_4]^{2+}$ core should be much easier to oxidise than $[Ru(II)(bpy)_2]^{2+}$, i.e. the transition behaves as LMCT instead of MLCT.

iv) The photoelectron spectrum of the ruthenium atom in these quinone species shows a core energy lying roughly between that expected for Ru(II) and that for Ru(III) [2].

These observations prompted the more detailed analysis of these species, reviewed in this Report.

4. $[Ru(bpy)_2(R_2\text{-}L,NH.NH)]^{2+}$ Series (II) [9]

The X-ray structure of the $[Ru(bpy)_2(L(NH.NH))]^{2+}$ ion [13] has bond distances consistent with the view [14] that it should be formulated $[Ru(III)(bpy)_2Sq(NH.NH)]^{2+}$. The electronic spectrum of this species (Figure 3) shows a low energy weak band which is identified with the overlap forbidden transitions $a_1, a_2 \longrightarrow 2b_2{}^*$ [9]. Analysis of a series of these complexes with varying substituent R in the benzoquinonediimine ring proved illuminating.

Figure 4 shows how the electrochemical potentials vary with R. The most salient observation is that the dependence of the first oxidation potential upon R, as identified by its total Hammett $\Sigma\sigma_p$ value, is essentially parallel to the dependence of the first reduction potential.
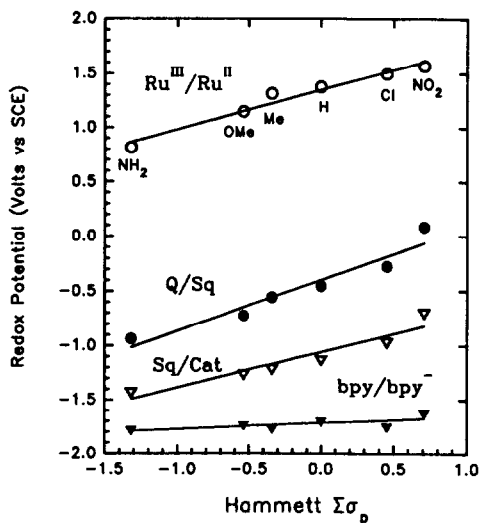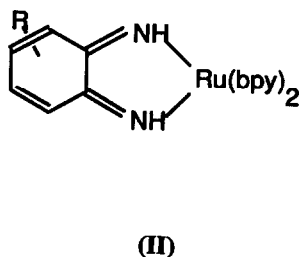

(II)

Figure 4. Behaviour of the redox processes of $[(bpy)_2Ru(R\text{-}L(NH.NH))]^{2+}$ species as a function of total Hammett $\Sigma\sigma_p$. The descriptions of processes as shown are the limits in the absence of mixing.

In the limiting [Ru(II)Q] description of the molecule, the first oxidation potential corresponds to Ru(III)/Ru(II) and the first reduction potential, to Q/Sq. However the parallel nature of these dependencies suggests considerable mixing between metal and ligand orbitals, possibly to a 50:50 extent [16]. Under such circumstances it is appropriate to argue that the species is best represented as $[Ru(III)(bpy)_2(Sq(NH.NH))]^{2+}$. We therefore explore the experimental consequences of 50:50 mixing between metal and ligand b_2 orbitals.

Figure 5 shows how the three observed electronic transitions behave as a function of substituent. The a_1,a_2 orbitals (see Figure 2) behave as largely metal, giving rise to the Ru (a_1,a_2) ---> π^*bpy MLCT transition (band III(NH.NH)) shifting to the blue as the acceptor character of the quinonediimine ligand increases, while the Ru (a_1,a_2) ---> $2b_2^*$ (Band I) transition shifts to the red as a typical MLCT transition. Band II(NH.NH), however, b_2 ---> $2b_2^*$, shows little dependence upon $\Sigma\sigma$, if anything shifting to the blue like an LMCT transition. The scatter is real given the narrowness of the band and hence accuracy of measurement. Resonance Raman excitation into Band II(NH.NH) (Figure 6) shows a single very intense feature at 603 cm^{-1} (R = 4,5-Cl$_2$) corresponding with the ν(Ru-N) vibration; no internal quinonoid vibrations are excited.
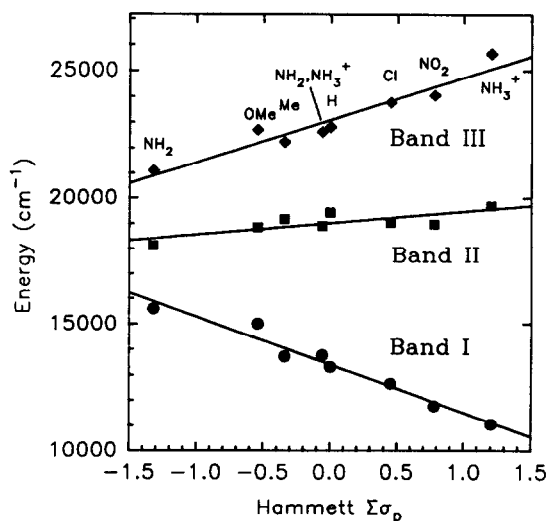

Figure 5. Behaviour of Bands I, II and III(NH.NH) with the Hammett $\Sigma\sigma$ value, as a function of substituent, as shown, for the species $[(bpy)_2Ru(R_2\text{-}L(NH.NH))]^{2+}$ dissolved in acetonitrile (except for R = 4,5-NH$_2$,NH$_3^+$, and R = 4,5-(NH$_3$)$_2^{2+}$ in 3M HCl and concentrated sulfuric acid respectively). The species with R = NO$_2$ is a mono 4-NO$_2$ substituted species.

A weak peak at ca 1204 cm^{-1} may be the first overtone of the $v(\text{Ru-N})$ vibration; if so, its observation requires there to be quite significant distortion of the Ru-N bond. The absence of internal quinone modes and the intense $v(\text{Ru-N})$ mode show that this transition involves distortion only of the Ru-N and that there is little net charge transfer to the quinonediimine ligand.

Indeed the proposal of ca 50:50 mixing between the metal d_{yz} and ligand LUMO π^* orbital, generating the b_2 (bonding) and $2b_2^*$ (anti-bonding) orbitals provides a rationale for the above observations. Such mixing would lead to no net electron transfer in the $b_2 \longrightarrow 2b_2^*$ transition, but would involve significant distortion in the Ru-N bond because this transition is effectively a $\pi \longrightarrow \pi^*$ transition within the Ru-N bond. Further, there would be no dependence upon the substituent, R, except for possible changes in the reorganisation energy terms.

Let us therefore explore whether the scatter seen for Band II in Figure 5 can be due to such variations in reorganisation energy. To a first approximation, the bandwidth at $1/e$ of the peak height of the relevant absorption band, $2\sigma^2$, is related to the frequencies, ω_k, and displacements, Δ_k of coupled vibrations, through the following equation [17]:

$$2\sigma^2 = \Sigma \Delta_k^2 \omega_k^2 \qquad\qquad (3)$$

The displacement parameter Δ_k is a dimensionless measure of the change in the kth coordinate between ground and excited state.
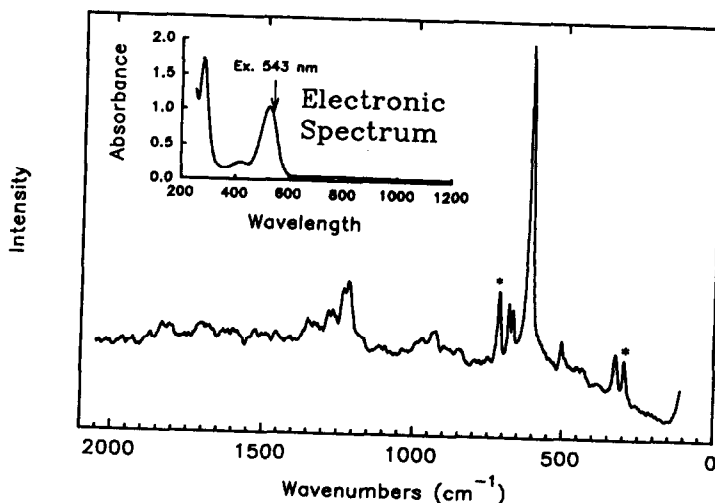

Figure 6. The resonance Raman spectrum of $[(\text{bpy})_2\text{Ru}(4,5\text{-Cl}_2\text{L(NH.NH)})]^{2+}$ dissolved in dichloromethane and excited at 543 nm.

Since the inner reorganisation energy can be written as a sum over $K_q \Delta_k^2$, where K_q is the force constant of the bond, the bandwidth and reorganisation energy are closely related. Since only one vibration, the Ru-N stretching vibration near 600 cm^{-1}, is excited, this model predicts a correlation between the scatter in Figure 5, and the variation in bandwidth for Band II, and the Ru-N stretching frequency (in the absence of force constant data), as a function of $\Sigma\sigma_p$. This indeed seems to be the case (Figure 7).

Thus the proposal of approximately 50:50 mixing of metal and ligand character, in the b_2 and $2b_2*$ orbitals, is likely. The MLCT behaviour observed with Band I, suggests rather less mixing of metal and ligand functions in the a_1 and a_2 orbitals. With the approximation of pure metal character for these orbitals, and 50:50 mixing (strong coupling) in b_2 and $2b_2*$, the formal valence bond description of this series of compounds is $[Ru(III)(bpy)_2(Sq(NH.NH))]^{2+}$ as indeed proposed by Carugo [14].
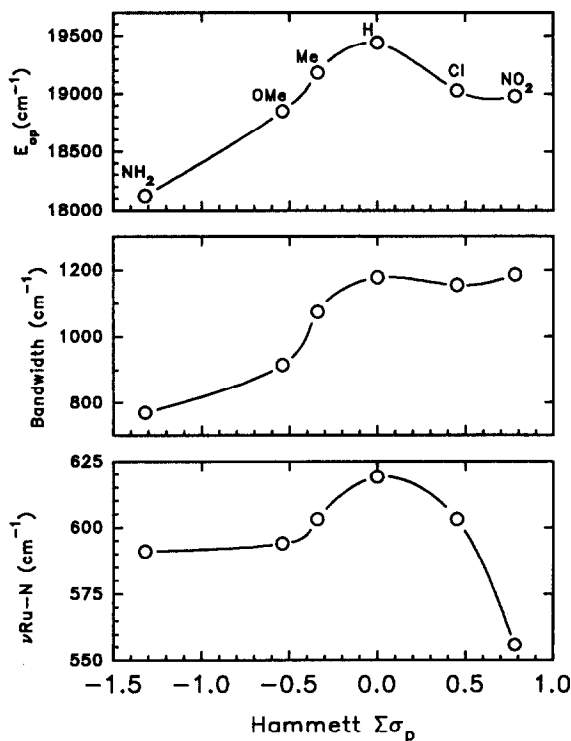

Figure 7. Spectroscopic data for $[(bpy)_2Ru(R_2\text{-}L(NH.NH))]^{2+}$ species, as a function of substituent. Upper: optical transition energy of Band II(NH.NH); middle: bandwidth at 1/e of the height of Band II(NH.NH); lower: v(Ru-N) stretching frequencies. For R see Figure 5.
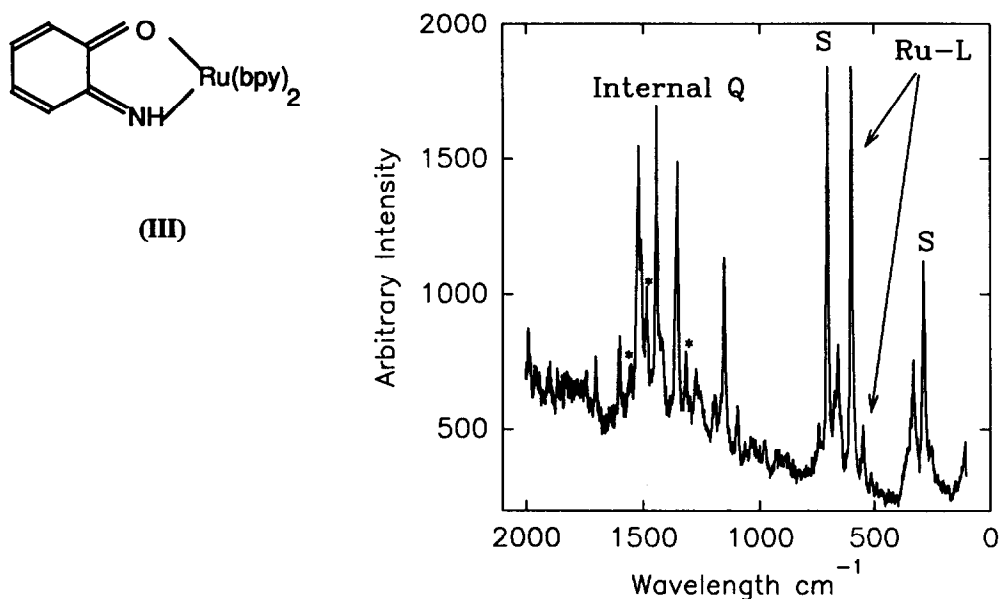
Figure 8. The resonance Raman spectrum of $[(bpy)_2Ru(L(NH.O))]^{2+}$, in dichloromethane, excited at 488 nm. Peaks with an asterisk are bipyridine vibrations.

5. $[Ru(bpy)_2(L(NH.O))]^{2+}$ (III) [9,18]

This species is evidently not a "simple average" of the L(NH.NH) and L(O.O) species since its electronic spectrum is obviously different (Figure 3). There are at least two fairly strong transitions in the 470 - 600 nm range, near 495 (Band II(NH.O)) and 566 nm (Band I(NH.O)).

Figure 8 shows a resonance Raman spectrum for this species, exciting at 488 nm, and shows enhancement of internal quinone deformations in the region 1300 - 1600 cm^{-1} and two ruthenium ligand stretching vibrations at 548 and 598 cm^{-1}. Figure 9 shows how the intensities (relative to a solvent vibration) of the two ruthenium ligand vibrations, and two of the internal quinone modes, varies with the excitation frequency through the two electronic transitions.

Consideration of the data in Figure 9 reveals that the band at 495 nm (Band II) is

coupled to the Ru-L stretching mode at 598 cm^{-1} and to internal quinone modes at 1154, 1356, 1444, 1522 and 1603 cm^{-1}, with the intensity of the Ru-L vibration being slightly more than that of the strongest internal quinone mode. This behaviour contrasts with
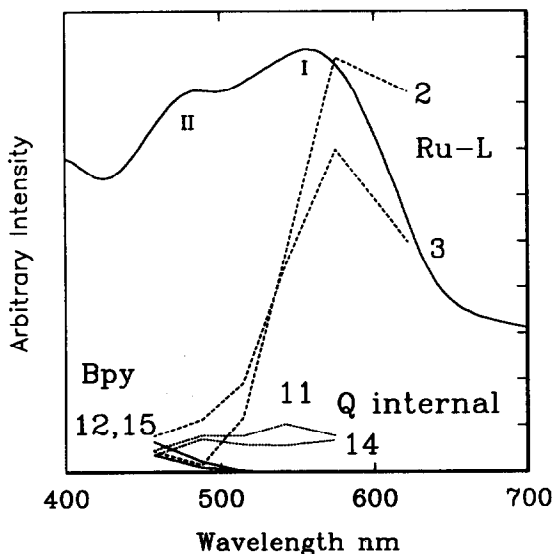

Figure 9. Excitation profile for a selection of the enhanced vibrations for [(bpy)$_2$Ru(Q(NH.O))]$^{2+}$ in dichloromethane, with the electronic spectrum superimposed thereon. Peaks 12,15 are bipyridine vibrations, 11 and 14 are internal quinone coordinates and 2 and 3 are Ru-L coordinates.

that for the band at 566 nm (Band I(NH.O)) which couples strongly to both Ru-L modes. The enhancement of the internal quinone modes are the essentially the same for both transitions, implying they terminate on the same orbital. However they differ in the relative enhancement of the Ru-L vibration being very much larger for the 548 cm^{-1} peak coupled to the 566 nm Band I(NH.O).

We expect to observe two transitions in parallel with the development above, and with that described below for species IV. The intense Band I(NH.O) shows enhancement primarily of the Ru-L modes and is readily assigned to d$_{yz}$ ---> π^* Q (using the same reference frame as for species I). However the d$_{xy}$ ---> π^* Q transition is expected to lie at lower energy than Band I(NH.O); it is therefore difficult to associate it with Band II(NH.O). Rather we tentatively propose that Band II(NH.O) is the ligand $\pi(a_2)$ ---> π^* Q, being a transition from what was the ligand HOMO but which may be substantially mixed with d$_{xy}$.

This orbital will less strongly coupled to the metal, than d_{yz}, and hence transition therefrom causes less distortion in the Ru-L coordinates.

6. [Ru(bpy)$_2$(dadib)]$^{2+}$ (IV) [19].

The presence of the diaminophenyl substituent on the benzoquinonediimine fragment confers some interesting additional properties which may be used to probe electronic structure. The electronic spectrum of this species, Figure 10, depends markedly on the solvent (solvatochromism), especially upon its hydrogen bond donor or acceptor character. Band I(dadib) shifts to higher energy with increasing hydrogen bond donor character of the solvent (equivalent to increasing Lewis acidity), and in the limit (e.g. in water, or in the presence of acid or BF$_3$) Band I(dadib) is obscured under Band II(dadib).

It is probably much weaker under these circumstances, though we note that the total integrated intensity of both bands remains roughly constant. A plot of the energy of Band I(dadib) versus a function of the Taft and Kamlet hydrogen bond donor and acceptor parameters is linear (see inset Figure 10).
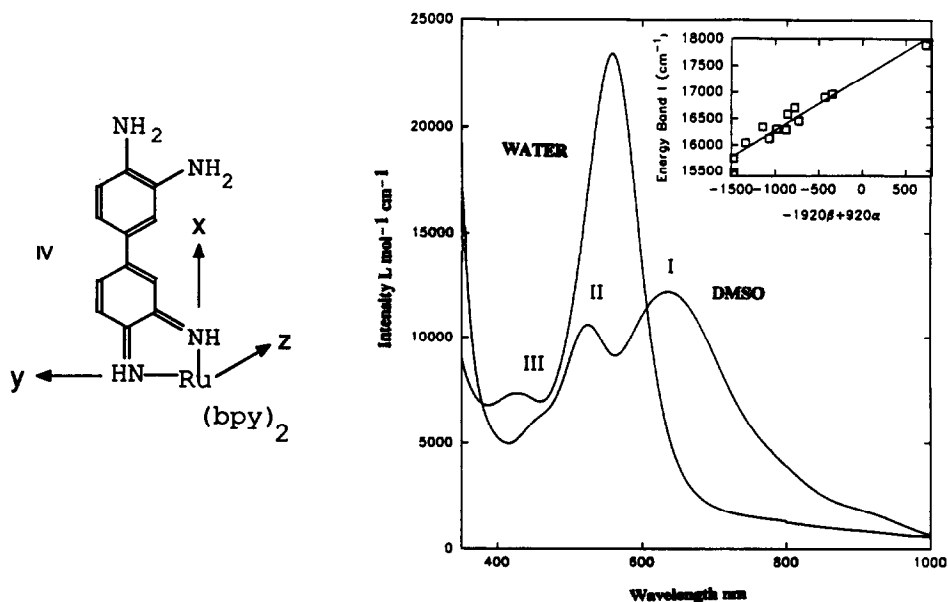

Figure 10. The electronic spectra of [Ru(bpy)$_2$(dadib)]$^{2+}$ dissolved in water and dimethylsulfoxide, as indicated. The inset shows a plot of energies of Band I(dadib) in a range of solvents, versus the Taft and Kamlet hydrogen bond donating and acceptor parameters, α and β, [19].

The resonance Raman spectrum (in water and in DMSO) shows two Ru-NH= vibrations, at 575 and 618 cm^{-1}, associated with the two chemically different NH groups, one, labelled p-NH, para to the diaminophenyl ring, and the other, labelled m-Nh, meta to the diaminophenyl ring. An excitation profile is shown, for a DMSO solution, in Figure 11. One Ru-NH is in strong resonance with Band II(dadib), and the other with Band I(dadib). Further, internal quinonediimine resonances are enhanced with excitation in Band I(dadib), but to a much lesser degree under the higher energy Band II(dadib). This behavior is strikingly different from that described above for the L(NH.O) system even though the local symmetry about the ruthenium atom is similar in the two systems.

AM1 and ab initio calculations [19] show that the solvatochromism arises through variation in twisting at the 1,1' connection. In the twisted form, (two rings perpendicular) charge separation between the two ends of the molecule is maximised and is favoured by binding a Lewis acid or hydrogen bond donor species, e.g. water, H$^+$, BF$_3$ etc at the diamino end of the molecule. Placing a Lewis base (hydrogen bond acceptor) at the diamino end, favours a flattening of the molecule, with greater participation of canonical form V, to distribute charge over the whole molecule. These effects are offset by H-H interactions at the 1,1' site which would cause the molecule to twist in the absence of other perturbations.
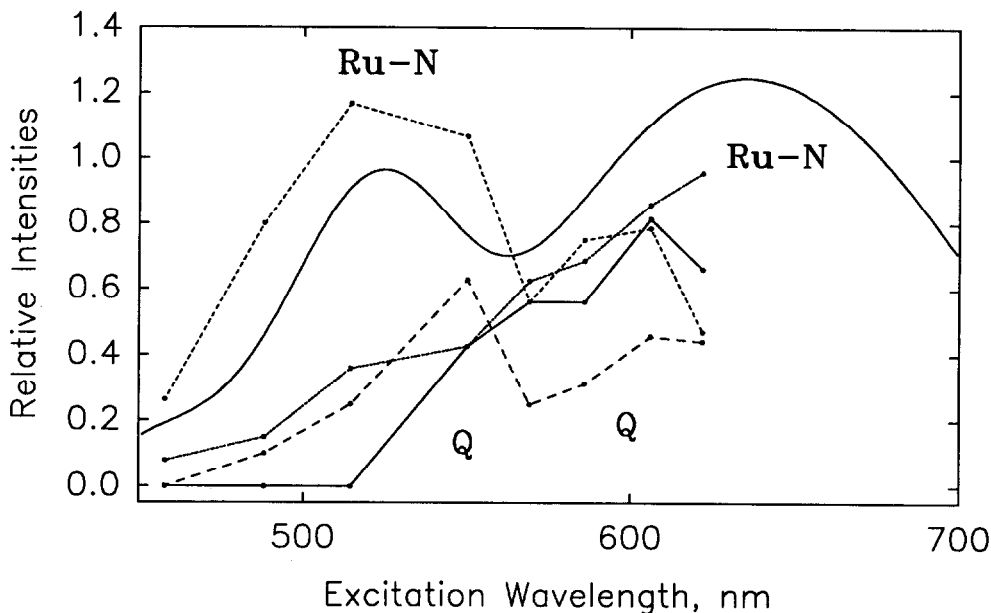

Figure 11. An excitation profile for [Ru(bpy)$_2$(dadib)]$^{2+}$ dissolved in DMSO, showing internal quinonediimine and Ru-NH coordinates, as labelled [19].

The solvatochromism plot shown in Figure 10 (inset) then reflects variation in twist angle as a function of the hydrogen bond donor or acceptor character of the solvent. A characteristic property of the dadib system is that certain molecular orbitals display a highly asymmetric electron density distribution such that, in a given orbital, there may be charge on one NH group with little or none on the other NH group, or vice versa. It is therefore inappropriate to consider this molecule to have effective C_{2v} symmetry as used for the other R-L,NH.NH systems.

Thus, based upon AM1 calculations of (F_2B)dadib, electron density distributions are as follows (dealing here only with the two imino groups):-

	Flat	Twisted
HOMO-1	π,m-NH only	no charge on imino NH end of molecule
HOMO	π,almost entirely on m-NH	no charge on imino NH end of molecule
LUMO	π^* (both NH) (b_2 in C_{2v})	π^* (both NH) (b_2 in C_{2v})

In summary, the LUMO in both the twisted and flat forms has rather similar electron density on both imino groups and therefore effective C_{2v} symmetry through the diiminobenzene ring fragment, but the HOMO in the flat form has density almost entirely on the m-HN= group. It is therefore appropriate to use C_s symmetry and align the x and y axes with the two NH groups (as shown in IV). In these circumstances the MO diagram (Figure 12) shows the interaction of HOMO and HOMO-1 with d_{xz}, and of the LUMO with both d_{xz} and d_{yz}. The two observed transitions are then readily identified as follows:

Band I(dadib) d_{xz} ---> π^*, and Band II(dadib) d_{yz} --> π^*

As the molecule changes from twisted to flat, charge builds up on the meta HN= residue causing the d_{xz} orbital energy to increase and thus Band I red shifts as the molecule becomes flatter (e.g. in DMSO). As the molecule twists, charge is lost from the m-NH site, and since there is also no charge on the p-NH= site in the HOMO and HOMO-1, the molecule assumes effective C_{2v} symmetry in which the second Ru-Q transition is overlap forbidden; hence Band I(dadib) weakens and we only observe Band II(dadib). Transitions from the HOMO (above d_{yz} in Figure 12), and from the d_{xy} orbital, to π^* are expected to be weak.
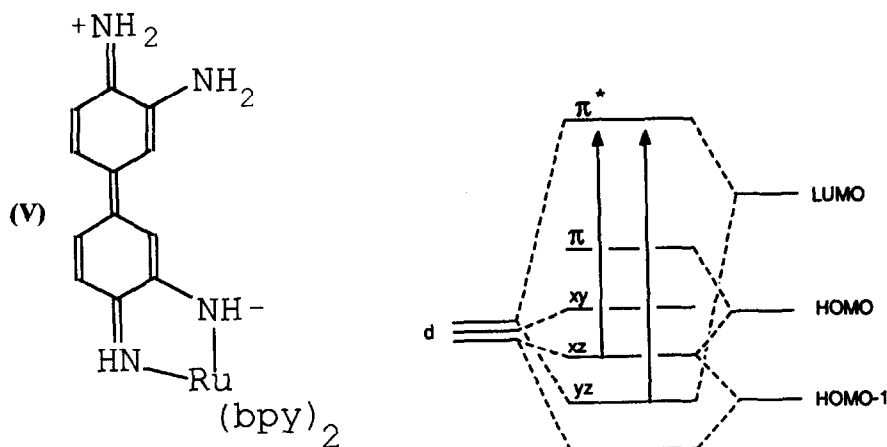
Figure 12. An M. O. diagram for $[Ru(bpy)_2(dadib)]^{2+}$ showing assignments of the two principal absorption bands [19].

7. Concluding Remarks

The four systems under investigation here, while fairly closely related, have shown quite disparate behaviour as the coordinating group is changed from oxygen to nitrogen, and as the local symmetry changes. This study reveals how a detailed study can teach us a lot about the subtle effects of changing symmetry upon electronic coupling, electron distributions, and effective oxidation states. Comparatively few such studies of metal complexes containing redox active ligands have been undertaken. The results discussed here suggest that this is an area rich for future discovery.

8. Acknowledgements

9. References

1. M. A. Haga, E. S. Dodsworth and A. B. P. Lever, Inorg. Chem., **1986**, 25, 447.
2. A. B. P. Lever, P. R. Auburn, E. S. Dodsworth, M. Haga, M. Melnik and W. A. Nevin, J. Am. Chem. Soc., **1988**, 110, 8076.
3. M. A. Haga, E. S. Dodsworth, A. B. P. Lever, S. R. Boone, and C. G. Pierpont J. Am. Chem. Soc., **1986**, 108, 7413.
4. P. R. Auburn, E. S. Dodsworth, M. Haga, W. Liu, W. A. Nevin, and A. B. P. Lever, Inorg. Chem., **1991**, 31, 3502.
5. S. Bhattacharya, and C. G. Pierpont, Inorg. Chem., **1992**, 31, 35.
6. S. Bhattacharya, and C. G. Pierpont, Inorg. Chem., **1991**, 30, 2906.
7. S. Bhattacharya, and C. G. Pierpont, Inorg. Chem., **1991**, 30, 1511.
8. M. A. Haga, K. Isobe, S. R. Boone, and C. G. Pierpont, Inorg. Chem., **1990**, 29, 3795.
9. H. Masui, P. R. Auburn and A. B. P. Lever, Inorg. Chem., 30, 2402. (1991).
10. D. J. Stufkens, Th. L. Snoeck and A. B. P. Lever, Inorg. Chem., 27, 953-956 (1988).
11. S. D. Pell, R. B. Salmonsen, A. Abelleira and M. J. Clarke, Inorg. Chem., **1984**, 23, 385.
12. E.S. Dodsworth and A. B. P. Lever, Chem. Phys. Lett., **1986**, 124, 152.
13. P. Belser, A. von Zelewsky, and M. Zehnder, Inorg. Chem. **1981**, 20, 3098.
14. O. Carugo, K. Djinovic, M. Rizzi and C. B. Castellani, J. Chem. Soc. Dalton Trans., **1991**, 1551.
15. H. Masui, A. B. P. Lever and E. S. Dodsworth, Inorg. Chem. **1993**, 32, 0000.
16. G. A. Mines, J. A. Roberts, and J. T. Hupp, Inorg. Chem., **1992**, 31, 125; R. De la Rosa, P. J. Chang, F. Salaymeh and J. C. Curtis, Inorg. Chem., **1985**, 24, 4229.
17. L. Tutt, L. and J. I. Zink, J. Am. Chem. Soc. **1986**, 108, 5830.
18. H. Masui, A. B. P. Lever and D. J. Stufken, in preparation.
19. R. A. Metcalfe, E. S. Dodsworth, A. B. P. Lever, and W. J. Pietro, Inorg. Chem., submitted 1992.